

CushionCatch: Compliant Catching Mechanism for Mobile Manipulators via Combined Optimization and Learning

Bingjie Chen[†], Keyu Fan[†], Houde Liu, Chongkun Xia, Liang Han, Bin Liang

Abstract—This paper presents a framework to achieve compliant catching with cushioning mechanism (CCCM) for mobile manipulators. First, we introduce a two-level motion optimization scheme, comprising a high-level capture planner and a low-level joint planner. The low-level joint planner consists of two distinct components: Pre-Catching (PRC) planner and Post-Catching (POC) planner. Next, we propose a network that leverages the strengths of LSTM for temporal dependencies and positional encoding for spatial context (P-LSTM). P-LSTM is designed to effectively learn compliant control strategies from human demonstrations. To account for structural differences between humans and robots, safety constraints are incorporated into POC planner to avoid potential collisions. We validate the CCCM framework through both simulated and real-world ball-catching scenarios, achieving a success rate of 98.70% in simulation, 92.59% in real-world tests, and a 33.2% reduction in impact torques.

I. INTRODUCTION

Manipulating dynamic objects is challenging, requiring a sophisticated interplay of object detection, motion planning, and control [1]. In dynamic manipulation scenarios, tasks such as throwing [2], [3], juggling [4], and catching [5], [6] are essential. Catching dynamic objects requires quick and precise motion planning, followed by fast and accurate execution. For the motion planning of catching, the process can be divided into two phases, Pre-Catching (PRC) and Post-Catching (POC) [7]. In the POC phase, for a high-stiffness robot, the object may bounce away or generate significant impact forces upon contact. To address this, incorporating a cushioning mechanism during catching is beneficial, as it reduces impact forces [8], [9], prevents damage to both the robot and the object [10], and minimizes the risk of rebound, especially for high-speed or high-mass objects [11], [12]. Moreover, since humans naturally exhibit cushioning

This work was supported by National Natural Science Foundation of China (No.62203260, 92248304), The Shenzhen Science Fund for Distinguished Young Scholars (RCJC20210706091946001), Guangdong Young Talent with Scientific and Technological Innovation (2019TQ05Z111), Tsinghua SIGS Cross Research and Innovation Fund (JC2021005). († indicates equal contribution) (Corresponding authors: Houde Liu; Chongkun Xia)

Bingjie Chen, Keyu Fan and Houde Liu are with the Center for Artificial Intelligence and Robotics, Shenzhen International Graduate School, Tsinghua University, Shenzhen 518055, China. (cbj23@mails.tsinghua.edu.cn, fky23@mails.tsinghua.edu.cn, liu.hd@sz.tsinghua.edu.cn)

Chongkun Xia is with the School of Advanced Manufacturing, Sun Yat-Sen University, Shenzhen 518055, China. (xiachk5@mail.sysu.edu.cn)

Liang Han is with the School of Electrical and Automation Engineering, Hefei University of Technology, Hefei 230009, China. (lianghan@hfut.edu.cn)

Bin Liang is with the Navigation and Control Research Center, Department of Automation, Tsinghua University, Beijing 100084, China (bliang@tsinghua.edu.cn).

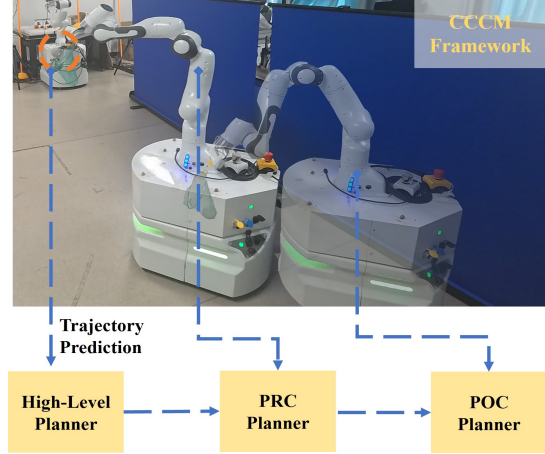


Fig. 1: The mobile manipulator’s motions under CCCM framework when catching a ball.

behavior when catching objects, an effective approach would be for the robot to learn this motion from humans.

Mobile manipulators are particularly adept at dynamic manipulation tasks, outperforming conventional stationary robots [13], [14] with greater flexibility and efficiency [15], [16], [17]. Their mobility allows them to actively navigate and interact with objects [18], [19]. In catching tasks, most prior research focused on rigid control approaches, often overlooking the importance of compliant control [1], [6], [14], [20]. Mobile manipulators, with their wireless capabilities, are ideal for learning human-like compliant behavior. We focus on introducing a framework for compliant catching using human demonstration data, which is designed to be modular, allowing easy integration with other robotic systems.

Compared with previous works, the contributions of this letter are:

1. Propose a two-level optimization scheme that includes a high-level capture planner and a low-level joint planner. This scheme addresses all planning and tracking challenges during the POC and PRC phases, while also solving potential safety concerns arising from structural differences in imitation learning.

2. Propose a P-LSTM network, a sequence-to-sequence model that combines a Long-Short-Term Memory network (LSTM) with positional encoding to predict commands, enabling the effective learning of compliant control strategies from human demonstrations.

3. Simulation and physical experiments were conducted on a mobile manipulator to validate the effectiveness of

the CCCM framework and the role of compliance. Catching success rates of 98.70% in simulation, 92.59% in physical experiments and a 33.2% reduction in impact torque were achieved.

II. RELATED WORK

Many studies have examined ball catching with fixed-base manipulators [1], [6], [21], [22], focusing particularly on motion planning for the manipulator. Early research utilized heuristic methods to determine optimal grasping points and generated motion trajectories through interpolation. However, these methods often fall short of achieving the most effective capture motion of the robot. A more effective approach involves using nonlinear optimization to identify the optimal joint configuration for catching the ball, along with parameterization techniques such as five-order polynomials [20].

Imitation learning allows algorithms to learn from human demonstrations, simplifying the acquisition of complex behaviors [23]. [7] creates nucleated motion primitives from human demonstration data to generate compliant trajectories. [24] uses a Gaussian Mixture Model and a Long-Short Term Memory (LSTM) model to predict the trajectory of a manipulation. However, their approach does not account for the potential safety issues arising from structural differences between humans and robots.

III. MODELING AND PROBLEM FORMULATION

A. System Model

The mobile manipulator we use includes a mobile base and a manipulator, with $n = n_b + n_m$ degrees of freedom. The state of the manipulator is described by joint positions $\mathbf{q}_m \in \mathbb{R}^{n_m}$. For a mobile base with a differential drive, we use the full location description (x_b, y_b, φ) and define the $\mathbf{q}_b = (\varphi, d)^T$ as virtual joints, where $d = \sqrt{x_b^2 + y_b^2}$.

For the container fixed at the end for catching the ball, we get the overall position positive kinematic as follows:

$${}^c\mathbf{T} = {}^w\mathbf{T}(x_b, y_b, \varphi) \cdot {}^b\mathbf{T} \cdot {}^m\mathbf{T}(\mathbf{q}_m) \cdot {}^e\mathbf{T} \quad (1)$$

where w, b, m, e, c represent the world, mobile base, manipulator base, end-effector, and container coordinate system, respectively.

Analogous to the Jacobian used in manipulator kinematics, we define the extended Jacobian matrix ${}^w\mathbf{J}$ for the mobile manipulator to compute the container's velocity in the world coordinate system.

$${}^w\mathbf{v} = {}^w\mathbf{J}(x_b, y_b, \varphi, \mathbf{q}_m, {}^e\mathbf{T})\dot{\mathbf{q}} \quad (2)$$

where $\dot{\mathbf{q}} = (\dot{\mathbf{q}}_b, \dot{\mathbf{q}}_m)^T$ and ${}^w\mathbf{v} = (v_x, v_y, v_z, \omega_x, \omega_y, \omega_z)^T$. This maps the velocity of whole-body joints to the container's velocity.

The flying ball is treated as a point mass influenced by aerodynamic drag and gravity [25]. The equation governing the ball's motion can be described as:

$$\ddot{\mathbf{p}} = -\mathbf{g} - k_{ad}\|\dot{\mathbf{p}}\|\dot{\mathbf{p}} \quad (3)$$

where \mathbf{p} is the ball's position in the world frame, $\mathbf{g} = [0, 0, g]^T$ is the gravitational acceleration, k_{ad} is the aerodynamic drag coefficient and $\|\cdot\|$ is the Euclidean norm.

B. Problem Formulation

1) *Problem 1:* Catching a moving ball requires that the container and the ball align in both position and direction. Thus, the goal of catching the ball at the catch time t_{ca} can be achieved by satisfying the following two conditions:

$${}^w\mathbf{P}(\mathbf{q}_{ca}) = \mathbf{p}(t_{ca}) \quad (4)$$

$$\frac{{}^w\mathbf{z}(\mathbf{q}_{ca})}{|{}^w\mathbf{z}(\mathbf{q}_{ca})|} = -\frac{\dot{\mathbf{p}}(t_{ca})}{|\dot{\mathbf{p}}(t_{ca})|} \quad (5)$$

where ${}^w\mathbf{P}$ denotes the position of the container in the world frame, \mathbf{q}_{ca} is the joint configuration of the robot at the catch time t_{ca} , ${}^w\mathbf{z}(\mathbf{q}_{ca})$ indicates the container's z-axis vector expressed in the world frame.

2) *Problem 2:* Given the catch configuration \mathbf{q}_{ca} , we should start with trajectory planning from q_0 . Once the ball is caught, the planning transitions to a compliant control strategy. The two phases, Pre-Catching (PRC) and Post-Catching (POC) can be described as:

$$\begin{cases} \Phi_{prc}(t; T_{prc}, \mathbf{q}_0, \mathbf{q}_{ca}), & t < t_{ca} \\ \Phi_{poc}(t; \mathbf{q}, \psi), & t \geq t_{ca} \end{cases} \quad (6)$$

where T_{prc} denotes the trajectory planning time of PRC; ψ represents the output of the compliant control strategy.

3) *Problem 3:* Given the sequence of ball's velocity $\dot{\mathbf{p}}(t_{ca})$ and position $\mathbf{p}(t_{ca})$ before catching, we need to predict the expected compliant sequence ψ of the manipulator to catch the ball with a cushioning mechanism. This can be formulated as follows:

$$\psi = \mathbf{N}(\mathbf{p}(t_{ca}), \dot{\mathbf{p}}(t_{ca})) \quad (7)$$

where $\mathbf{N}(\cdot)$ means prediction network.

IV. METHODOLOGY

A. Ball Estimation and Prediction

To predict the trajectory of a ball in flight, we first estimate its current state and then use a dynamical model to forecast its future position over a given time horizon. We use a modified discrete-time Kalman filter that accounts for aerodynamic drag, as described in [25]. Given measurements at the discrete time index k , the state of the ball at the next time step $\mathbf{p}[k+1|k]$ can be predicted as follows:

$$\ddot{\mathbf{p}}[k|k] = -\mathbf{g} - k_{ad}\|\dot{\mathbf{p}}[k|k]\|\dot{\mathbf{p}}[k|k] \quad (8a)$$

$$\dot{\mathbf{p}}[k+1|k] = \dot{\mathbf{p}}[k|k] + \delta_k\ddot{\mathbf{p}}[k|k] \quad (8b)$$

$$\mathbf{p}[k+1|k] = \mathbf{p}[k|k] + \delta_k\dot{\mathbf{p}}[k|k] + \frac{1}{2}\delta_k^2\ddot{\mathbf{p}}[k|k], \quad (8c)$$

where δ_k is the interval time between k and $k+1$. The Kalman filter we used follows the standard approach described in [26]. The aerodynamic drag coefficient k_{ad} is estimated offline using a Recursive Least-Squares estimator [25]. Then the ball's trajectory $\hat{\mathbf{p}}$ can be predicted by (3) through numerically integrating over a finite time horizon. We use a cubic spline interpolation between two-time steps to query the $\hat{\mathbf{p}}(t)$ and $\dot{\hat{\mathbf{p}}}(t)$ at any time.

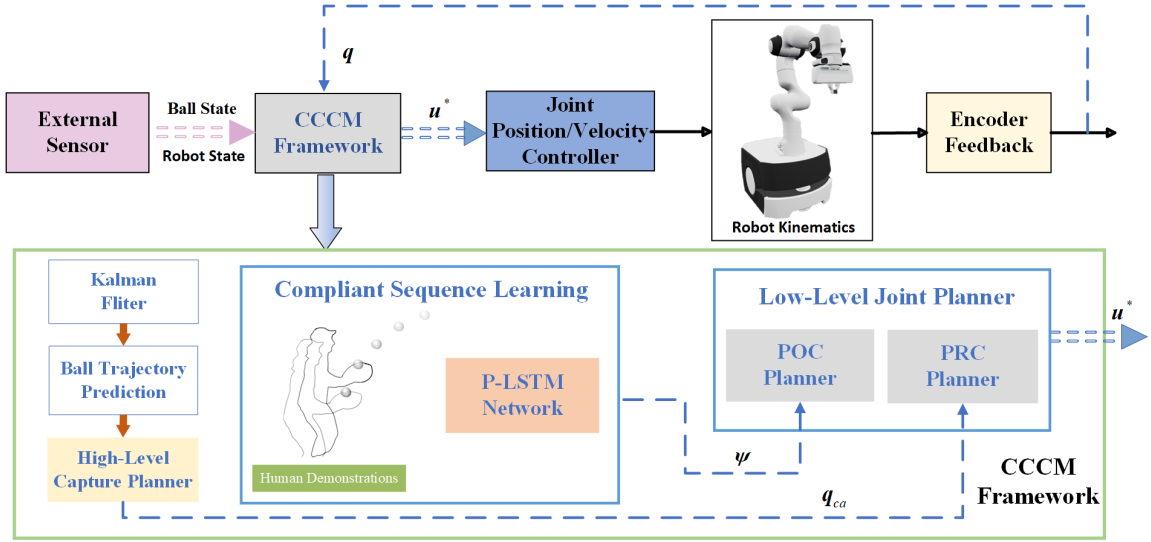


Fig. 2: Overview of the system framework: External sensors provide status for both the ball and the robot. The ball's state is refined using a Kalman filter, which is then used to predict its future trajectory over a time horizon. The high-level capture planner computes the optimal capture state, \mathbf{q}_{ca} . The PRC planner generates rapid motion trajectories for \mathbf{q}_{ca} and sends them to the joint position controller. The POC planner tracks the compliant velocity sequence from the P-LSTM network, which is designed to learn from human demonstrations.

B. High-Level Capture Planner

The high-level planner outputs an optimal catching configuration \mathbf{q}_{ca} and catch time t_{ca} that enables the container to intercept the ball's trajectory at time t_{ca} . For this purpose, the following QP problem is formulated:

$$\min_{\mathbf{q}_{ca}, t_{ca}} \frac{1}{2} (\mathbf{A} \|\mathbf{q}_{ca} - \mathbf{q}_0\|^2 - \alpha \|t_{ca}\|^2) \quad (9a)$$

$$\text{s.t. } {}^w\mathbf{P}(\mathbf{q}_{ca}) = \hat{\mathbf{p}}(t_{ca}) \quad (9b)$$

$$\frac{{}^w\mathbf{z}(\mathbf{q}_{ca})}{|{}^w\mathbf{z}(\mathbf{q}_{ca})|} = -\frac{\hat{\mathbf{p}}(t_{ca})}{|\hat{\mathbf{p}}(t_{ca})|} \quad (9c)$$

$${}^w\mathbf{T}_z(\mathbf{q}_{ca}) \geq \beta \quad (9d)$$

$$\mathbf{q}_{ca}^{min} \leq \mathbf{q}_{ca} \leq \mathbf{q}_{ca}^{max} \quad (9e)$$

The objective function tends to minimize joint movement and extend capture time. \mathbf{A} and α are the weights associated with each aspect. \mathbf{A} can be defined as:

$$\mathbf{A} = \begin{pmatrix} \mathbf{E}(\Lambda_b) & \mathbf{0} \\ \mathbf{0} & \mathbf{E}(\Lambda_m) \end{pmatrix} \quad (10)$$

where \mathbf{E} represents identity matrix, Λ_b , Λ_m denotes the cost values associated with the mobile base and the manipulator. Due to the motion control accuracy of the mobile base is generally lower than the manipulator, Λ_b tends to set higher than Λ_m to encourage more movement of the manipulator.

${}^w\mathbf{T}_z(\mathbf{q}_{ca})$ in (9d) denotes the Z-axis height of the container at the capture configuration \mathbf{q}_{ca} . For the potential collision between the mobile base and the manipulator, [14], [27] use a semi-cylindrical spatial constraint for the position of the container. However, we find that the manipulator typically extends to reach out for a catching. Therefore, by ensuring the height of capture, such a self-collision will also be prevented. Moreover, due to the subsequent PRC phase, it is meaningful for the robot to maintain a specific height

when catching the ball. The constraint of ${}^w\mathbf{T}_z(\mathbf{q}_{ca})$ is simple but reasonable and effective.

C. Low-Level Joint Planner

1) *PRC Planner*: In the high-level capture planner, it provide the joint configuration of the robot to catch the ball. For the catching task, ensuring both speed and smoothness in trajectory planning is essential. Considering the maximum acceleration and speed limits for each joint, we determine the minimum trajectory planning time for each joint, denoted as t_{prc} :

$$t_{prc} = \begin{cases} 2\sqrt{\frac{\Delta q}{\ddot{q}_{max}}}, & \Delta q < 2\Delta q_{acc} \\ 2\frac{\dot{q}_{max}}{\ddot{q}_{max}} + \frac{\Delta q - \dot{q}_{max}(\frac{\dot{q}_{max}}{\ddot{q}_{max}})^2}{\ddot{q}_{max}}, & \Delta q \geq 2\Delta q_{acc} \end{cases} \quad (11)$$

where $\Delta q = |\mathbf{q}_{ca} - \mathbf{q}_0|$, $q_{acc} = \frac{1}{2}\ddot{q}_{max} \left(\frac{\dot{q}_{max}}{\ddot{q}_{max}}\right)^2$. This calculation assumes that the joint accelerates to maximum speed using the maximum acceleration and then maintains that speed until the deceleration phase. While such an extreme motion is not used in practice, this simplified method helps us quickly estimate the duration of the joint movement. Then, we can define the time parameter T_{prc} of PRC as follow:

$$T_{prc} = \lambda \cdot \max(t_{prc}^i), \quad i \in [1, n] \quad (12)$$

where $\lambda > 1$ is a proportion parameter to enlarge planning time appropriately. Then, we can get the PRC planner in (6):

$$\Phi_{prc} = \text{Poly5}(t; T_{prc}, \mathbf{q}_0, \mathbf{q}_{ca}) \quad (13)$$

where $\text{Poly5}()$ represents a Quintic Polynomial Planning that maps the time t (ranging from 0 to T_{prc}) to the joint position based on the inputs $T_{prc}, \mathbf{q}_0, \mathbf{q}_{ca}$.

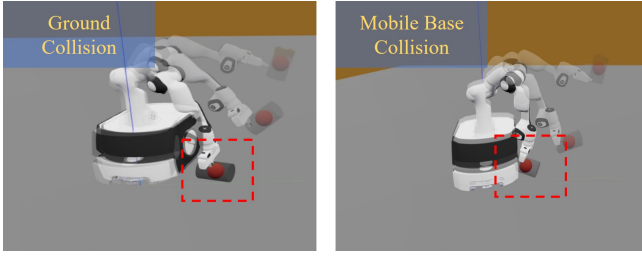


Fig. 3: The collision occurs when there are no safety constraints in the POC planner.

2) *POC Planner*: After the robot catches the ball, it needs to apply compliant control to have a cushioning mechanism. Given the velocity-compliant sequence ψ produced by the network, we need to track this sequence. Additionally, to ensure safety, we must consider potential collisions between the mobile base and the manipulator, as well as between the manipulator and the ground. Therefore, we look at how Control Barrier functions(CBF) can encode safety constraints. The POC planner can be expressed as follows:

$$\Phi_{poc} = \min_{\dot{q}} \frac{1}{2} (\|\dot{q}\|^2 + \|\delta\|^2) \quad (14a)$$

$$\text{s.t. } {}^w \mathbf{J} \dot{q} = \psi_i + \delta \quad (14b)$$

$$\dot{f}(z_c) \cdot {}^w \mathbf{J}_z \cdot \dot{q} \geq -\gamma_z f(z_c) \quad (14c)$$

$$\dot{g}(x_c, y_c) \cdot {}^w \mathbf{J}_{xy} \cdot \dot{q} \geq -\gamma_{xy} g(x_c, y_c) \quad (14d)$$

where ψ_i represents the i -th sequence of ψ and δ is the slack vector. The components of the Jacobian in z -axis and the x, y -axis are denoted by ${}^w \mathbf{J}_z$ and ${}^w \mathbf{J}_{xy}$. The function $f(z_c)$ represents the safe distances between the container and the ground. And $g(x_c, y_c)$ is the safe horizontal distance between the container and the mobile base. Safety is maintained when $f(z_c) > 0$ and $g(x_c, y_c) > 0$. In the optimization problem above, equality constraints ensure the container keeps track of expectations ψ . To ensure safety, Control Barrier Functions (CBFs) are used as inequality constraints, which help maintain safe forward invariance [28], [29]. Although the compliant sequence learned from human demonstrations may indicate potential collisions, these are effectively mitigated through the implementation of safety constraints. By imposing limits on the container's height along the z -axis and regulating its horizontal distance from the base, the optimization process filters out potential collisions while minimizing deviations from the desired trajectory. This ensures safety without compromising performance. The collision scenarios are shown in Figure 3.

D. Compliant Sequence Learning

Given the velocity and position states of the object before catching, we employ the P-LSTM network to achieve accurate predictions for the sequences required for compliant control. We focus on tracking the complaint velocity sequence (14b) due to the limitations in the sampling space for position components, which might not cover the full range. On the contrary, the relativity of speed can be better generalized.

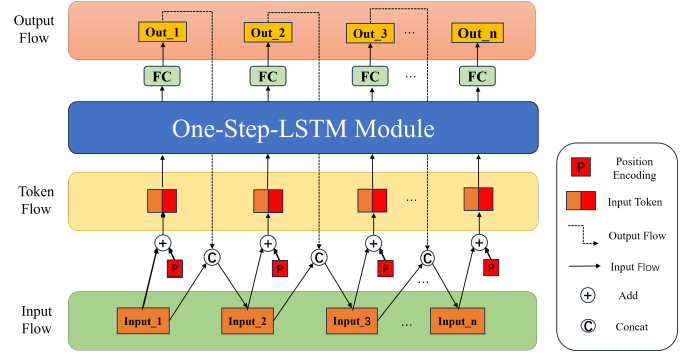


Fig. 4: P-LSTM network for compliant sequence learning from human demonstrations

Specifically, we concatenate the initial six-dimensional input sequence (comprising position and velocity along the x, y, z -axes) into a variable denoted as $input_1$. This serves as the first input at time step 1. This concatenated vector is then input into a one-step LSTM module, which consists of an LSTM cell followed by a fully connected layer that projects the hidden state to the output dimension. Then, the first output out_1 is produced at time step 1 by the one-step LSTM. Subsequently, we concatenate $input_1$ and out_1 as the second input $input_2$ at time step 2 and again put it into the same one-step-LSTM module to get the second output flow out_2 at time step 2. This process repeats until the maximum sequence length is reached.

To incorporate the positional order of the input sequences, similar to the approach in [30], we apply position encoding in our LSTM model. Specifically, we encode the sine and cosine of the input position sequence and combine these encodings with the input data. The resulting position-encoded input tokens are then passed into the LSTM model, preserving the order information between sequences for improved learning performance. As shown in Fig. 4, the overall output flow can be described as:

$$input_i = input_{i-1} \oplus out_{i-1} + PE(i-1, 6) \quad (15a)$$

$$out_i = \mathbf{G}(input_i) \quad (15b)$$

where $PE(\cdot)$ means positional encoding and i is the i -th time step, \oplus represents concatenation vertically and $\mathbf{G}(\cdot)$ is the one-step-LSTM module.

For each position l in the sequence, the positional encodings are calculated as follows:

$$pe(l, 2i, k) = \sin\left(\frac{l}{10000^{2i/k}}\right) \quad (16a)$$

$$pe(l, 2i+1, k) = \cos\left(\frac{l}{10000^{2i/k}}\right) \quad (16b)$$

$$PE(l, k) = pe(l, 0, k) | pe(l, 1, k) | \dots | pe(l, k, k) \quad (16c)$$

where $|$ means concatenation horizontally and k is the embedding dimension.

V. EXPERIMENTS

We evaluate our framework through experiments conducted both in simulation and on a physical mobile manip-

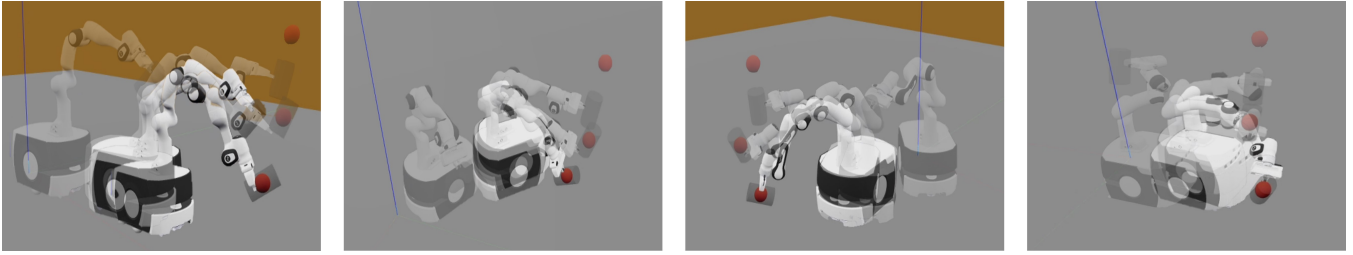


Fig. 5: Snapshots of some catching experiments in the simulation where robot opacity increased with time. It shows the ball approaching the robot from the front, right, left, and back, respectively.



Fig. 6: The robot motions under CCCM framework to catch a ball with compliant control. They represent the starting state of motion, the end state of PRC planner, and the end state of POC planner.

ulator. We use the following value for the parameters of our framework: $k_{ad} = 0.0295$ in (3); $\alpha = 2$ in (9a); $\beta = 0.5$ in (9d); $\Lambda_b = 5, \Lambda_m = 1$ in (10); $\lambda = 1.5$ in (12); $\gamma_z = 0.1$ in (14c); $\gamma_{xy} = 0.1$ in (14d). In P-LSTM, we set the hidden size to 64 and a fully connected layer block from 64 to 6. During training, we use mean square error(MSE) between predicted output and ground truth value, the learning rate is 0.001 and the max output sequence length is capped at 16.

A. Data Collection and Processing

We capture the velocity and position sequences of the ball using a NOKOV motion-capture device during human-catching demonstrations. These sequences cover a short period from just before the ball is caught until it comes to a complete stop. We identify the moment of catching by detecting the point with the highest average velocity variation across the x, y, z -axes. This point is then used to split the sequence into input data and corresponding output labels.

B. Simulation Scenarios

We use the Swift and Rtb Python libraries [31] as our simulated environments. Initially, we generated 6,000 ball samples $[p_x, p_y, p_z, \dot{p}_x, \dot{p}_y, \dot{p}_z]$, restricting their positions within a cylindrical space of a specified height. We ensured that their trajectories, for $t > 0.5$, would pass through the robot’s capture range. Then ball parameters are generated randomly by procedure. Additionally, we performed ablation studies on the collision avoidance constraints in (14c) and (14d) during the POC phase (2,000 pieces of data for each test). The statistical results are presented in Table I.

Fig. 5 shows the robot motions of some experiments where the ball comes from different directions. Table I demonstrates the results of 6000 random catching tasks, showing that the CCCM framework achieves a 98.70% success rate for catching. In practice, constraints (14c) and (14d) do not

TABLE I: Simulation Results Over 6000 Random Catching Tasks

Approach	Success Rate	Ground Crash	Base Crash	Not Catch
General	98.70%	0.00%	1.05%	0.25%
Without (14c)	82.80%	13.70%	3.20%	0.30%
Without (14d)	89.40%	0.00%	10.40%	0.20%

affect the PRC planner, resulting in similar “Not Catch” rates. However, incorporating collision avoidance constraints notably reduces the incidence of collisions. Without (14c) or (14d), the probability of collisions in their respective dimensions increases substantially.

C. Real-World Scenarios

As shown in Fig. 6, a real-world experiment is conducted on a mobile manipulator. We use a C-100 differential mobile base($n_b = 2$) and a franka panda manipulator($n_m = 7$), interfacing with the robot through ROS Noetic. NOKOV motion capture provides position and velocity measurements, which are used for both ball state estimation and mobile base state tracking. We use a standard tennis ball fitted with a reflective strip for tracking purposes. When a human hand throws the ball, a Kalman filter models the ball’s dynamics using feedback from the initial frames and updates the model in the subsequent few frames. This model is then used to predict the ball’s trajectory over the next 1.5s. Notably, due to the coupling effects of differential wheel steering, our high-level planner considers only the combined motion q_1 and restricts the differential motion q_0 to 0 to achieve more accurate tracking in the PRC. We conducted a total of 100 hand-throwing experiments. However, due to inaccuracies in hand throwing, 19 attempts clearly fell outside the robot’s capture range. Out of the remaining 81 valid throws, the robot successfully captured the ball 75 times, resulting in

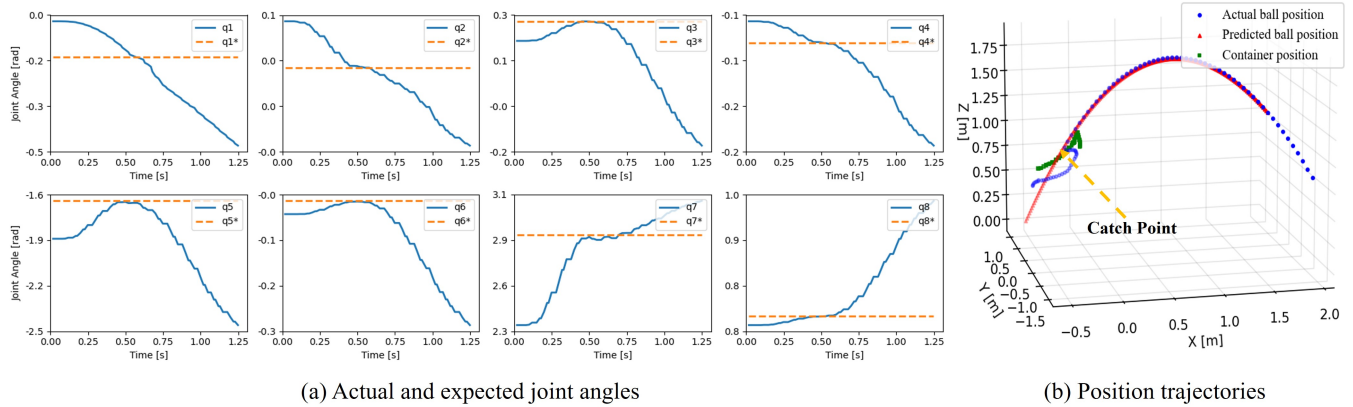


Fig. 7: The change of the joint angles of the robot during a catch, the expected joint angles calculated by the high-level planner, and the trajectory of the ball and the container. The catching time is $t_{ca} = 0.598$.

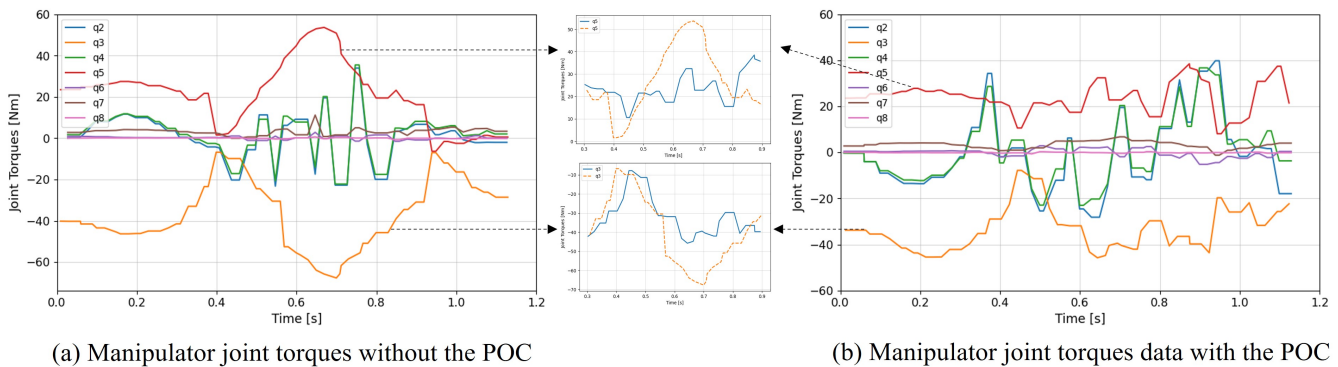


Fig. 8: Manipulator joint torques without and with the POC planner. The POC planner reduces the impact torques when robot catching.

a success rate of 92.59%, without any collision. The failure occurred because noise in the capture system caused a discrepancy between the filter’s estimated state and the actual state, leading to deviations in the predicted trajectory. In related systems [1], [20], large-scale data simulations were not conducted, yet we still outperformed them in real-world experiments. Additionally, we incorporated compliant behavior, making the system safer and more relevant.

Fig. 7(a) illustrates the expected output of the high-level capture planner and the changes in joint angles during the catching. The PRC planner successfully guided all joints to meet the expected positions before the capture time $t_{ca} = 0.598$ and the system transitioned smoothly into the POC planner phase. Fig. 7(b) shows the actual, predicted trajectory of the ball and the trajectory of the container during catching. The trajectory prediction is accurate. It is worth noting that the position of the container does not coincide with the ball’s position after the catch due to the depth of the net bag. Fig. 8(a) and Fig. 8(b) present the joint torque data without and with the POC planner, respectively. q_3 and q_5 are the main joints that receive impact in the process of catching. Clearly, the addition of the POC planner to have compliant catching significantly reduced the impact on the joints. By comparing the maximum torque of q_3, q_5 , the compliant strategy reduces the impact torques

by an average of 33.2%, demonstrating that the compliant strategy learned by the network is effective. At the same time, normal torque fluctuations in other joints are expected due to joint movements during the POC planner. Moreover, it is worth mentioning that there is no collision in the physical experiments. The safety is ensured through our POC planner when applying the compliant sequences learned from human demonstrations to the robot.

VI. CONCLUSIONS

We present a framework integrating optimization and learning to enable compliant catching with a cushioning mechanism for mobile manipulators. The framework employs a two-level motion optimization: a high-level capture planner to determine the robot’s optimal catching state, and a low-level joint planner with PRC and POC planner to generate rapid motions and track compliant sequences while ensuring safety, respectively. Compliant control strategies are learned through a P-LSTM network from human demonstrations, which leverage the strengths of LSTM for temporal dependencies and positional encoding for spatial context. Experimental results indicate a 98.70% success rate in simulations and 92.59% in real-world tests, alongside a 33.2% decrease in impact torque. Moreover, due to the modular design of the CCCM framework, we envision that it can be easily ported to other robots or fields.

REFERENCES

- [1] B. Bäuml, T. Wimböck, and G. Hirzinger, “Kinematically optimal catching a flying ball with a hand-arm-system,” in *2010 IEEE/RSJ International Conference on Intelligent Robots and Systems*, 2010, pp. 2592–2599.
- [2] Y. Liu, A. Nayak, and A. Billard, “A solution to adaptive mobile manipulator throwing,” in *2022 IEEE/RSJ International Conference on Intelligent Robots and Systems (IROS)*, Oct. 2022, pp. 1625–1632.
- [3] A. Takahashi, M. Sato, and A. Namiki, “Dynamic compensation in throwing motion with high-speed robot hand-arm,” in *2021 IEEE International Conference on Robotics and Automation (ICRA)*, 2021, pp. 6287–6292.
- [4] J. Z. Woodruff and K. M. Lynch, “Robotic contact juggling,” *IEEE Transactions on Robotics*, vol. 39, no. 3, pp. 1964–1981, Jun. 2023.
- [5] S. Kim, A. Shukla, and A. Billard, “Catching objects in flight,” *IEEE Transactions on Robotics*, vol. 30, no. 5, pp. 1049–1065, 2014.
- [6] S. S. M. Salehian, M. Khoramshahi, and A. Billard, “A dynamical system approach for softly catching a flying object: Theory and experiment,” *IEEE Transactions on Robotics*, vol. 32, no. 2, pp. 462–471, 2016.
- [7] J. Zhao, G. J. G. Lahr, F. Tassi, A. Santopaolo, E. De Momi, and A. Ajoudani, “Impact-friendly object catching at non-zero velocity based on combined optimization and learning,” in *2023 IEEE/RSJ International Conference on Intelligent Robots and Systems (IROS)*, Oct. 2023, pp. 4428–4435.
- [8] Y. Wang, N. Dehio, and A. Kheddar, “On inverse inertia matrix and contact-force model for robotic manipulators at normal impacts,” *IEEE Robotics and Automation Letters*, vol. 7, no. 2, pp. 3648–3655, 2022.
- [9] S. Haddadin, A. Albu-Schäffer, and G. Hirzinger, “Requirements for safe robots: Measurements, analysis and new insights,” *The International Journal of Robotics Research*, vol. 28, no. 11-12, pp. 1507–1527, Nov. 2009.
- [10] N. Uchiyama, S. Sano, and K. Ryuman, “Control of a robotic manipulator for catching a falling raw egg to achieve human-robot soft physical interaction,” in *2012 IEEE RO-MAN: The 21st IEEE International Symposium on Robot and Human Interactive Communication*, 2012, pp. 777–784.
- [11] S. Gholami, F. Tassi, E. De Momi, and A. Ajoudani, “A reconfigurable interface for ergonomic and dynamic tele-locomanipulation,” in *2021 IEEE/RSJ International Conference on Intelligent Robots and Systems (IROS)*, 2021, pp. 4260–4267.
- [12] T. Stouraitis, L. Yan, J. Moura, M. Gienger, and S. Vijayakumar, “Multi-mode trajectory optimization for impact-aware manipulation,” in *2020 IEEE/RSJ International Conference on Intelligent Robots and Systems (IROS)*, 2020, pp. 9425–9432.
- [13] A. Zeng, S. Song, J. Lee, A. Rodriguez, and T. Funkhouser, “Tossing-bot: Learning to throw arbitrary objects with residual physics,” *IEEE Transactions on Robotics*, vol. 36, no. 4, pp. 1307–1319, 2020.
- [14] R. Lampariello, D. Nguyen-Tuong, C. Castellini, G. Hirzinger, and J. Peters, “Trajectory planning for optimal robot catching in real-time,” in *2011 IEEE International Conference on Robotics and Automation*, May 2011, pp. 3719–3726.
- [15] G. Wang, W. Wang, P. Ding, Y. Liu, H. Wang, Z. Fan, H. Bai, Z. Hongbiao, and Z. Du, “Development of a search and rescue robot system for the underground building environment,” *Journal of Field Robotics*, vol. 40, no. 3, pp. 655–683, 2023.
- [16] M. Mashali, L. Wu, R. Alqasemi, and R. Dubey, “Controlling a non-holonomic mobile manipulator in a constrained floor space,” in *2018 IEEE International Conference on Robotics and Automation (ICRA)*, May 2018, pp. 725–731.
- [17] Z. Xie, L. Jin, X. Luo, M. Zhou, and Y. Zheng, “A biobjective scheme for kinematic control of mobile robotic arms with manipulability optimization,” *IEEE/ASME Transactions on Mechatronics*, vol. 29, no. 2, pp. 1534–1545, Apr. 2024.
- [18] G. Rizzi, J. J. Chung, A. Gawel, L. Ott, M. Tognon, and R. Siegwart, “Robust sampling-based control of mobile manipulators for interaction with articulated objects,” *IEEE Transactions on Robotics*, vol. 39, no. 3, pp. 1929–1946, 2023.
- [19] J. Pankert and M. Hutter, “Perceptive model predictive control for continuous mobile manipulation,” *IEEE Robotics and Automation Letters*, vol. 5, no. 4, pp. 6177–6184, 2020.
- [20] K. Dong, K. Pereida, F. Shkurti, and A. P. Schoellig, “Catch the ball: Accurate high-speed motions for mobile manipulators via inverse dynamics learning,” in *2020 IEEE/RSJ International Conference on Intelligent Robots and Systems (IROS)*, Oct. 2020, pp. 6718–6725.
- [21] M. M. Schill, F. Gruber, and M. Buss, “Quasi-direct nonprehensile catching with uncertain object states,” in *2015 IEEE International Conference on Robotics and Automation (ICRA)*, 2015, pp. 2468–2474.
- [22] U. Frese, B. Baumli, S. Haidacher, G. Schreiber, I. Schaefer, M. Hahnle, and G. Hirzinger, “Off-the-shelf vision for a robotic ball catcher,” in *Proceedings 2001 IEEE/RSJ International Conference on Intelligent Robots and Systems. Expanding the Societal Role of Robotics in the Next Millennium (Cat. No.01CH37180)*, vol. 3, 2001, pp. 1623–1629 vol.3.
- [23] M. Zare, P. M. Kebria, A. Khosravi, and S. Nahavandi, “A survey of imitation learning: Algorithms, recent developments, and challenges,” *IEEE Transactions on Cybernetics*, pp. 1–14, 2024.
- [24] R. Mori, T. Aoyama, T. Kobayashi, K. Sakamoto, M. Takeuchi, and Y. Hasegawa, “Real-time spatiotemporal assistance for micromanipulation using imitation learning,” *IEEE Robotics and Automation Letters*, vol. 9, no. 4, pp. 3506–3513, 2024.
- [25] M. Müller, S. Lupashin, and R. D’Andrea, “Quadcopter ball juggling,” in *2011 IEEE/RSJ International Conference on Intelligent Robots and Systems*, Sep. 2011, pp. 5113–5120.
- [26] T. D. Barfoot, *State Estimation for Robotics: Second Edition*, 2nd ed. Cambridge: Cambridge University Press, 2024.
- [27] B. Bäuml, T. Wimböck, and G. Hirzinger, “Kinematically optimal catching a flying ball with a hand-arm-system,” in *2010 IEEE/RSJ International Conference on Intelligent Robots and Systems*, Oct. 2010, pp. 2592–2599.
- [28] H. Zhang, Z. Li, and A. Clark, “Model-based reinforcement learning with provable safety guarantees via control barrier functions,” in *2021 IEEE International Conference on Robotics and Automation (ICRA)*, 2021, pp. 792–798.
- [29] R. Herguedas, M. Aranda, G. López-Nicolás, C. Sagüés, and Y. Mezouar, “Multirobot control with double-integrator dynamics and control barrier functions for deformable object transport,” in *2022 International Conference on Robotics and Automation (ICRA)*, 2022, pp. 1485–1491.
- [30] H. Kim, Y. Ohmura, and Y. Kuniyoshi, “Memory-based gaze prediction in deep imitation learning for robot manipulation,” in *2022 International Conference on Robotics and Automation (ICRA)*, 2022, pp. 2427–2433.
- [31] P. Corke and J. Haviland, “Not your grandmother’s toolbox—the robotics toolbox reinvented for python,” in *2021 IEEE International Conference on Robotics and Automation (ICRA)*. IEEE, 2021, pp. 11 357–11 363.